JOURNAL OF GEOPHYSICAL RESEARCH, VOL. 103, NO. B6, PAGES 12,321-12,338, JUNE 10, 1998

Hydrothermal circulation at the Cleft-Vance overlapping spreading center: Results of a magnetometric resistivity survey

Rob L. Evans,[1] Spahr C. Webb,[2] Marion Jegen[3,5] and Khamla Sananikone[4,6]

Abstract. We report on a magnetometric resistivity sounding carried out in the overlapping spreading center between the Cleft and Vance segments of the Juan de Fuca Ridge. The data collected reveal a strong three dimensionality in the crustal electrical resistivity structure on wavelengths of a few kilometers. Areas of reduced crustal electrical resistivities, with values approaching that of seawater, are seen beneath the neovolcanic zones of both active spreading centers. We interpret these reduced resistivities as evidence of active hydrothermal circulation within the uppermost 1 km of hot, young oceanic crust.

1. Introduction

Overlapping spreading centers (OSC) constitute an intermediate level of discontinuity in mid-ocean ridge spreading systems. They are found particularly on faster spreading ridges such as the East Pacific Rise (EPR) [*Lonsdale*, 1983; *Macdonald et al.*, 1984; *Kent et al.*, 1993], where they have a characteristic curved shape, with the tips of each spreading center curving inwards towards the other. An OSC typically has an overlap to offset aspect ratio of 3:1, with the lateral offset of the order of 5-10 km. OSCs found on the EPR also have an elliptical basin (of the order of a few hundred meters deep) in their center. Evidence of fossil basins away from the ridge appear to indicate that OSCs propagate along strike, with one segment capturing the other.

The OSC between the Cleft and Vance segments on the Juan de Fuca Ridge (JDF) is somewhat more enigmatic than those of the EPR. The Cleft segment, which is the southernmost of the system, has a morphology not unlike that of the fast spreading EPR. There is some seismic evidence of a magma chamber at a depth around 2.3 km [*Morton et al.*, 1987], and the northern end of the segment is known to have been recently volcanically active [*Embley and Chadwick*, 1994]. Recent volcanic activity has also been observed on parts of the Vance segment (Bob Embley, personal communication, 1996).

As well as being volcanically active, both northern Cleft and Vance were the sites of two large and anomalous hydrothermal megaplumes [*Baker et al.*, 1989], there is evidence of ongoing hydrothermal activity on the northern Cleft [*Embley and Chadwick*, 1994] and evidence of relic hydrothermal activity on Vance (Bob Embley, personal communication, 1996). Most of the heat lost through the seafloor at mid-ocean ridges does so through hydrothermal circulation. Hydrothermal circulation also plays an important role in the evolution of oceanic crust through processes of alteration and deposition [*Alt et al.*, 1986]. The magmatic budget of a mid-ocean ridge segment is a major contributor to the local thermal budget, yet despite this obvious tie between magmatism and hydrothermal activity, the spatial links and interplay between the two are not well understood. In fact, to date, there have been few constraints placed on the thermal state and physical properties of the upper crust by geophysical methods that are sufficient to determine patterns and modes of hydrothermal circulation. Critical unknowns are the depth extent, primary flow directions (i.e., along- or across-strike), and the degree to which flow is partitioned between low- and high-temperature regimes.

Most large-scale numerical models of ridge axis circulation have treated flow through a porous medium [e.g., *Sleep*, 1991; *Travis et al.*, 1991], with both two- and three-dimensional driving heat sources. These models feature flow which begins off-axis in a recharge zone, penetrates into the seafloor, and is drawn toward the ridge axis by magma-chamber driven convection. Hot fluids vent out in a narrow zone at the ridge axis, as required by numerous seafloor observa-

[1]Department of Geology and Geophysics, Woods Hole Oceanographic Institution, Woods Hole, Massachusetts

[2]Marine Physical Laboratories, Scripps Institution of Oceanography, La Jolla, California.

[3]Department of Physics, University of Toronto, Ontario, Canada.

[4]Department of Geology and Geophysics, Texas A&M University, College Station.

[5]Now at Institute of Theoretical Geophysics, Cambridge, England, United Kingdom.

[6]Now at U.S. Geological Survey, Woods Hole, Massachusetts.

Paper number 98JB00599.
0148-0227/98/98JB-00599$09.00

tions. A three-dimensional magma chamber can also initiate along-strike flow, although if the medium is regarded as isotropic, then there will be no preference between along- and across-strike flow.

Rosenberg et al. [1993] and *Haymon et al.* [1991] are advocates of along-axis flow, at least for the deep-penetrating, high-temperature component of discharge. They propose models in which the deep-penetrating fluids are confined to a narrow band beneath axis, while more pervasive, but lower temperature, circulation occurs within the uppermost extrusives. There is evidence from Deep Sea Drilling Project/Ocean Drilling Program (DSDP/ODP) hole 504B and from ophiolites of alteration within dikes [e.g., *Alt et al.*, 1986; *Nehlig and Juteau*, 1988; *Nehlig*, 1993], but both the porosity and permeabilities within the dike complex are low and possibly also anisotropic. *Rosenberg et al.* [1993] claim that fluid flow in dikes will be limited on the basis of borehole-derived permeability values of around 10^{-17} m^2. *Nehlig* [1993] also supports along-strike flow based on alteration patterns within the dike complex. In contrast, *Yang et al.* [1996] demonstrate that the presence of cracks, which have high internal permeabilities, can cause the initiation of subcritical convection in regions whose bulk permeability would otherwise be too small for convection to occur, resulting in significant across-strike flow.

Seismic velocities increase in the shallow crust with age owing to gradual cementation of cracks in the rocks with hydrothermal alteration, but seismology otherwise provides no constraints on the patterns of circulation within the crust. Deep-sea vent fields and their effluent plumes are the only observable evidence of the hydrothermal circulation in young ocean crust in unsedimented environments. However, the electrical resistivity in the fractured extrusives will be strongly influenced by temperature variations along and across strike, because the resistivity of the percolating seawater is strongly temperature dependent.

In this paper, we report on an electromagnetic survey using the magnetometric resistivity (MMR) sounding technique, which was completed across the Cleft-Vance OSC in June 1994. The experiment measured the electrical resistivity of the uppermost crust to a depth of about 1 km throughout the southernmost end of the OSC and NVZ of the Cleft and Vance segments. Magnetic fields generated by a vertical bipole source were measured by three seafloor magnetometers at 34 transmitter locations. Magnetic field amplitudes were measured to ranges of over 5 km, and we discuss and interpret models of electrical resistivity, which explain our data in terms of hydrothermal circulation beneath the OSC.

2. Northern Cleft Segment, Juan de Fuca Ridge

The JDF has an intermediate spreading rate of about 6 cm/yr. This is reflected by the ridge morphology, which is typical neither of the fast-spreading EPR nor of the slow-spreading Mid-Atlantic Ridge but which exhibits characteristics of both along its length.

The Cleft segment is the southernmost section of the JDF and runs from the Blanco Fracture zone at 44°27′N to the OSC with the Vance segment around 45°N-45°10′N (Figure 1). Cleft geology has been described in detail [*Embley et al.*, 1983; *Kappel and Ryan*, 1986; *Kappel and Normark*, 1987].

Cleft is about 80 km long and has an axial valley of about 80-100 m deep and about 1 km wide, although the morphology changes along its length. At the southernmost end, the axial valley has a 30-50 m wide, 10-30 m deep axial graben, which has a cleft like appearance, giving the segment its name. The cleft dies out at around 44°44′N. North of this site, the axial valley deepens and becomes more fissured. The NVZ can be followed northward along the crest of a small volcanic ridge to about 45°10′N.

The seismic velocity structure below layer 2A is poorly constrained along both the Cleft and Vance segments. A survey by *Morton et al.* [1987] shows a weak intermittent midcrustal reflector that they interpret as the top of an axial melt body in both segments. However, the depth to the body is poorly constrained because of the lack of a detailed refraction survey.

Recent sheet and pillow flows have been observed by side-scan sonar, deep tow cameras and a series of Alvin dives [*Embley and Chadwick*, 1994; *Chadwick and Embley*, 1994]. The northern portion of the Cleft and Vance segments were the sites of anomalous hydrothermal plumes, known as megaplumes, which were detected in the mid-1980s [*Baker et al.*, 1987, 1989]. These events had characteristics distinct from other hydrothermal plumes associated with the focused discharge of black smoker fluid. The events were in some cases short-lived, had large positive temperature anomalies, contained a large amount of heat energy and had peculiar chemical signatures. Follow up surveys of the seafloor identified a large young sheet flow and pillow flows in the same area as the megaplumes. The fresh sheet flow extends from 44°44.5′N to 44°59.5′N and lies at the foot of the western wall of the axial valley. A linear series of fresh pillow mounds extends 17 km northward from the sheet flow to about 45°09′N. The total volume of flows is about 0.05 km^3, and they are associated with a single fracture system. The root supply for the recent volcanism along this segment has been proposed to be a lateral dike intrusion from a buried magma supply situated below the sheet flow [*Embley and Chadwick*, 1994].

The northern end of the Cleft segment overlaps the adjacent Vance segment by a distance of 15-20 km, with a lateral offset of about 5 km (Figure 1). The OSC does not exhibit the characteristic exaggerated curved shape of OSCs on the EPR, but rather each segment retains its linear shape. The Vance segment undergoes an eastward change in strike south of 45°15′N. The band of hydrothermal outflow and young volcanics extends northward through the OSC.

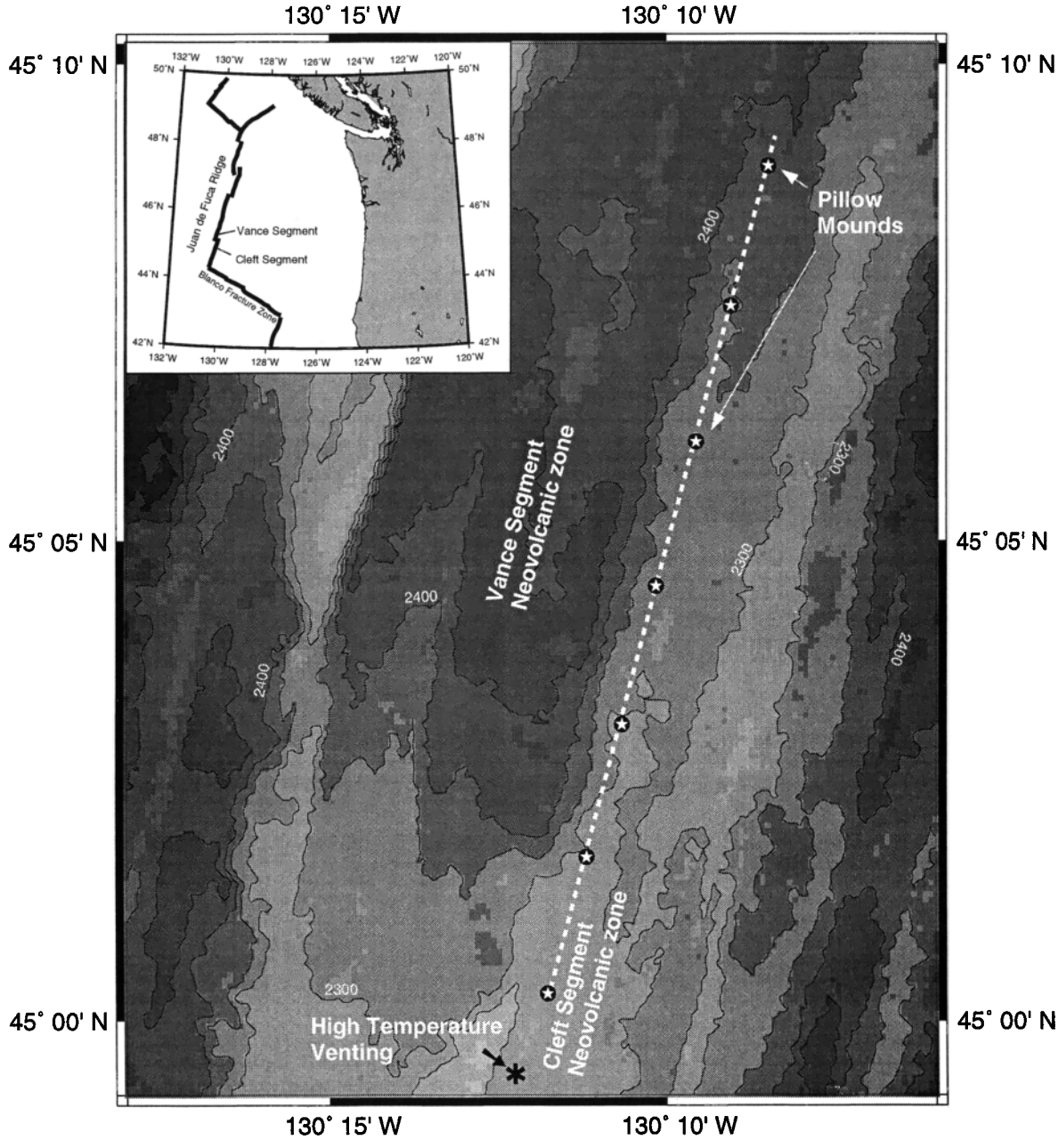

Figure 1. A bathymetric map of the Cleft-Vance OSC on the Juan de Fuca Ridge. Marked on the map are the positions of the Cleft and Vance neovolcanic zones (NVZ), the approximate position of the line of fresh pillow flows identified by *Chadwick and Embley* [1994], and the position of a known high-temperature hydrothermal vent. Water depths are shown in meters.

There is a change in ridge morphology from the Cleft to the Vance segments, with the Vance exhibiting a broad (5 km), 100 m deep steep-walled axial graben, with intermittent and en-echelon constructional volcanic mounds marking the NVZ. The axial valley is more extensively faulted than that of the Cleft. Recent volcanic activity has also been observed on parts of the Vance segment (Bob Embley, personal communication, 1996), with the freshest lavas found around 45°12′N on the largest volcanic edifice of the segment which stands some 100 m above the valley floor. Volcanic flows associated with the northernmost Cleft segment may cover the bounding fault of the eastern side of the Vance axial graben around 45°12′N (Bob Embley personal communication, 1996).

A seismic survey at the northern end of Cleft [*McDonald et al.*, 1994] featured air gun shots into ocean bottom seismometers with extensive azimuthal and range coverage used to identify crack-induced anisotropy within the shallowmost extrusive layer (seismic layer 2A). Also obtained were estimates of thickness variations in layer 2A. The thinnest region of extrusives was found in the axial valley of Cleft, coincident with the young sheet flow and documented hydrothermal activity. This is

consistent with models of crustal formation which place the thinnest zone of extrusives on axis at the locus of eruption, with subsequent thickening of the extrusives as the crust migrates away from the ridge [e.g., *Christeson et al.*, 1992]. The greatest variation in layer 2A thickness occurs within the overlapping rift zone. A broad zone of thick layer 2A (500 m) runs through the middle of the OSC, parallel to strike. Changes in extrusive layer thickness of about 300 m occur over lateral distances of a few kilometers. Layer 2A is generally thicker beneath the axis of the Vance segment than beneath Cleft.

Gravity measurements made within the OSC [*Stevenson et al.*, 1994] indicate the presence of low-density material beneath both limbs of the OSC. There are Bouguer anomaly lows at the southern end of the Vance segment as well as within the OSC which correlate with the thick layer 2A seen by *McDonald et al.* [1994]. On the basis of the density used to model the data collected, the shallow porosities across the OSC are on average 17%, but may be as high as 30% in places. However, reasonable shallow density variations do not adequately model the gravity signature across the OSC, and so there may be a deeper source of low-density material: possibly partial melt. Furthermore, the northern Cleft segment is mapped seismically as a region of thin layer 2A, while gravity data indicate low crustal densities, a contradiction that also requires further explanation besides changes in shallow porosity.

Tivey [1994] has completed sea surface, deep tow and submersible-based magnetic surveys across the Cleft-Vance OSC and also further north across the Vance segment. The axis of the northern Cleft segment is marked by a distinct magnetic anomaly low, explained by a thin magnetic source layer, in contrast to the Vance segment which requires a thick source layer. Magnetic source layer thickness seems to be well correlated with the layer 2A thickness variations reported by *McDonald et al.* [1994], indicating that the primary source of magnetic signal is probably fresh extrusive lavas.

3. MMR Method

In recent years, a variety of electrical methods have been developed for marine surveying purposes. Despite the many different experimental techniques used, the aim of all seafloor electrical experiments is essentially the same: to identify the electrical resistivity structure of some part of the seafloor, either in the crust or underlying mantle. Full details of the methods used can be found in the references cited below. An overview of marine electromagnetic techniques is given by *Chave et al.* [1991]. This paper reports on the results of one particular method known as MMR sounding, which has been successfully used on the seafloor in previous experiments [*Edwards et al.*, 1981; *Wolfgram et al.*, 1986; *Nobes et al.*, 1986, 1992].

The MMR method is a magnetic technique and involves two components: a source which is a vertical bipole and receivers which are remote seafloor magnetometers. The geometry of the system is shown in Figure 2. The method is essentially galvanic and does not rely on the inductive processes of other controlled source electromagnetic (EM) techniques [*Young and Cox*, 1981; *Cox et al.*, 1986, *Evans et al.*, 1991, 1994]. Yet, whereas other galvanic, or resistivity, techniques have poor sensitivity to the structure of a resistive seafloor, the MMR method is capable of identifying the seafloor resistivity, even when the source-receiver offset is short, of the order of the water depth. This enhanced sensitivity was demonstrated by *Wolfgram et al.* [1986], who compared a small MMR system with the traditional Wenner resistivity method.

In the presence of a layered seafloor, the magnetic field generated by the bipole source possesses an azimuthal symmetry and falls off with distance from the source approximately as $1/r^2$. If the current transmitted is known, then the amplitude of the magnetic field at sites remote to the source can be used to estimate the bulk electrical resistivity of the seafloor. The full expression for the azimuthal magnetic field at the seafloor is given by *Edwards et al.* [1981]. Experience has shown that the depth of resolution of the technique is about 1/3 the maximum source-receiver offset, limited by the pattern of current flow through the seafloor.

The magnetic field measured remotely to an MMR bipole source depends on the total current entering the seafloor through an Ampère circuit centered on the source and passing through the receiver. Because of this integrative nature, the magnetic field is sensitive only to large-scale features, which have dimensions that are a significant fraction of the source-receiver offset.

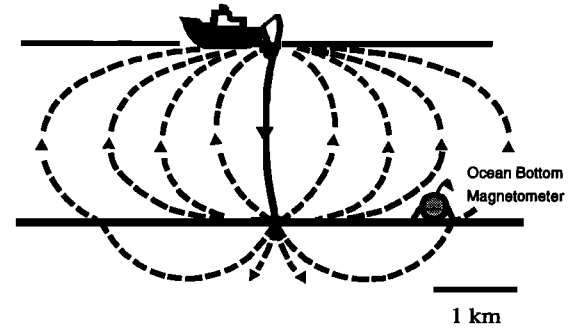

Figure 2. A schematic of the MMR method which features a vertical bipole source of current and a remote seafloor magnetometer. The vertical bipole creates a magnetic field which, over a uniform seafloor, possesses azimuthal symmetry. If the current passing through the wire and the source-receiver distance are known, then the strength of the seafloor magnetic field is diagnostic of the subseafloor electrical resistivity. A perfectly resistive seafloor would not allow the entry of current, and the seafloor magnetic field would be zero, by Ampère's law.

This facet means that the measurements are not influenced by the small-scale heterogeneities, which can have a large impact on electric field amplitudes [*Evans et al.*, 1991, 1994].

4. Resistivities of Hydrothermal Fluids

The electrical resistivity of the uppermost crust at the mid-ocean ridge depends primarily on the amount of seawater penetrating it but depends also on how the fluid is distributed [*Archie*, 1942; *Becker*, 1985; *Pezard*, 1990; *Evans et al.*, 1994; *Evans*, 1994]. A well-connected network of fluid-filled cracks will provide an optimal pathway for electrical conduction, and hence the resistivity will be low. An empirical relationship between measured resistivity (ρ_m), porosity (ϕ), and the resistivity of seawater (ρ_f) is *Archie*'s [1942] law

$$\rho_m/\rho_f = \phi^{-t}$$

This expression is the most commonly used estimator of porosity from electrical measurements in the oceanic crust [e.g., *Becker*, 1985]. Archie's law assumes that the solid phase contributes nothing to the overall conduction process, a reasonable assumption since the resistivity of basalt is several orders of magnitude higher than that of seawater. For a well-connected network of fluid-filled cracks, the exponent t in Archie's law approaches 1.2 [*Evans*, 1994].

From ambient seafloor temperatures to around 300°C, the resistivity of seawater decreases nearly linearly with temperature from 0.3 Ωm (3 S/m) to around 0.04 Ωm (25 S/m) [*Nesbitt*, 1993; *Quist and Marshall*, 1968], with little pressure dependence. The decreasing resistivity is primarily the result of increases in ionic mobilities. Above 350°C, the behavior of resistivity changes, becoming approximately proportional to density, and increases rapidly with increasing temperature. The critical point of seawater occurs about 500-600 m beneath the seafloor at a temperature of around 410°C [*Bischoff and Rosenbauer*, 1985]. Seawater filled crust at temperatures hotter than about 400°C will be electrically resistive regardless of its porosity.

Several models have been proposed which detail the thermodynamic state of seawater within the hydrothermal regime. For circulation above appropriate magma body depths between 1.5 and 1.8 km below the seafloor [*Kent et al.*, 1993] it seems unlikely that fluids are heated much above 400°C, at least in an openly circulating system in which cool seawater mixes with hydrothermal fluids [*Bischoff and Rosenbauer*, 1985; *Delaney et al.*, 1987; *Nehlig*, 1993]. There is evidence of magmatic fluids found as inclusions in gabbro and quartz-breccia and metabasalt samples from the Mid-Atlantic Ridge (where confining pressures are higher because of increased water depths) [*Kelley et al.*, 1993]. These inclusions show thermal histories involving temperatures in excess of 700°C. *Nehlig* [1993] suggests a model whereby these magmatic fluids are sandwiched in a reaction zone above the magma chamber and below an openly circulating system. In any event, these magmatic fluids are likely to be fairly resistive and at the low porosities expected for this part of the crust will not have a measurable electrical signature. However, fluids with temperatures in the range from 200°C to 350°C will have a strong effect on crustal resistivity.

To demonstrate the kinds of anomaly we might measure, we have calculated an expected resistivity depth cross section (Figure 3). The thermal structure (Figure 3a) is based on convection solutions for a porous medium [*Wilcock*, 1997]. We have converted the nondimensional temperatures to real values using a basal temperature of 500°C. Crustal porosities are estimated using values from, for example, *Becker* [1989] and *Stevenson et al.* [1994] (Figure 3b). The model is useful as it demonstrates the kind of signal we might expect to see above a region of convective upwelling. We have calculated resistivities for these thermal/porosity profiles using *Archie*'s [1942] law with an exponent of 1.2 (i.e., assuming a well interconnected fluid network).

The model shows a substantial resistivity anomaly within the upper 500-600 m of crust as a result of raised fluid temperatures (Figure 3c). This anomaly essentially tracks the head and periphery of the upwelling region, where porosities are moderately high but also where fluid temperatures are lower than about 400°C. If a uniform porosity of 5% is considered (Figures 3d and 3e), then the pattern of resistivity mimics the temperature solution, and while crustal values are low, they do not drop below 1.0 Ωm. It is important to note that the horizontal scale length of conductive anomaly is of the order of 500 m to 1 km, despite the fact that the central upwelling portion of convection is narrower (approximately 200-400 m). It is also important to note that our choice of porosity and thermal structures are by no means unique: they serve only to demonstrate the strong links between hydrothermal convection and electrical structure that can be exploited by the MMR method.

5. Effects of Buried Conductors

We have run simple forward model calculations to demonstrate the effects that buried conductive bodies have on MMR data. The modeling uses a finite difference scheme based on the algorithms of *Adams* [1989, 1991] to solve iteratively for the seafloor magnetic field. The code has been tested against analytic-layered solutions and is found to be accurate to about 10% in terms of apparent resistivity. The principal aim of the modeling is to demonstrate the sensitivity of the method to regions of anomalously conductive crust: this anomalous conductivity could be due to either hot seawater or partial melt, although here we focus our discussion on the effects of hydrothermal cells (conductive bodies).

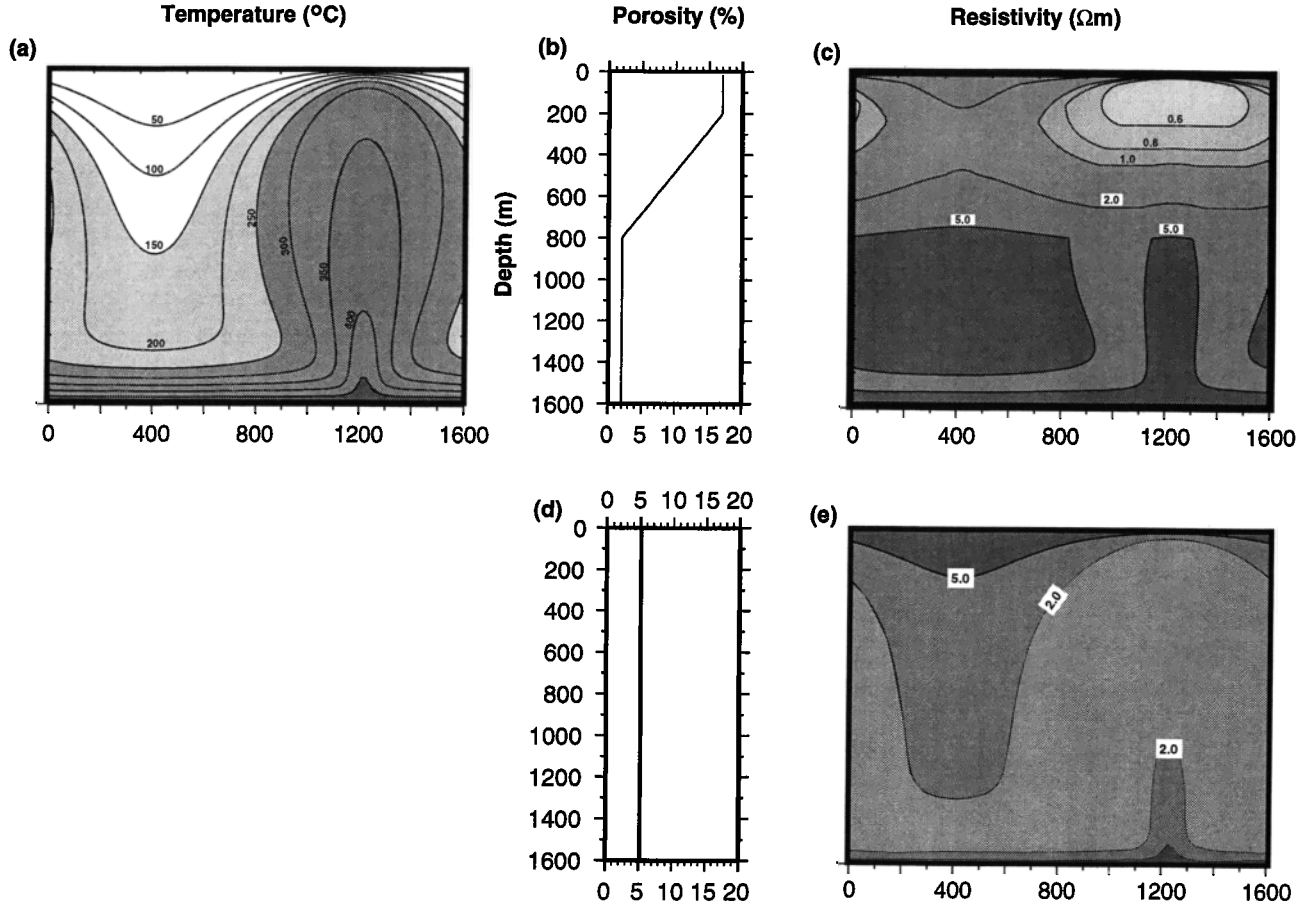

Figure 3. Ridge porosity and temperature structures which have been used to compute electrical resistivity cross sections. (a) The thermal structure is a porous medium convection solution with a basal temperature of 500°C [*Wilcock*, 1997]. We have scaled this solution approximately to a ridge with a magma chamber at 1.6 km. (b) We have considered a porosity profile based on the literature [*Becker*, 1989]. (c) A predicted resistivity cross section for the porosity profile in Figure 3b using Archie's law with an exponent of 1.2. The primary feature is the large region of low resistivity within the upper 500-600 m of seafloor. This figure demonstrates that while the convection model features a fairly focused upwelling, the electrical structure is impacted over a wider region of seafloor, away from the highest upwelling temperatures. (d) A uniform porosity of 5% explicitly shows the effect of temperature on bulk resistivity with (e) a large area of relatively low resistivities.

We have tested two models: one based loosely on the resistivity cross section in Figure 3c and one in which the resistivity anomaly is less extreme in amplitude and extends over the upper 1200 m of seafloor. Both models consider two anomalies centered beneath a ridge axis. Each anomaly is 1 km by 1 km, and they are located 1 km apart from each other (2 km center to center) along strike.

We have calculated the seafloor magnetic field that would be measured by four seafloor receivers and which is generated by a movable transmitter: fifty different transmitter locations were treated, giving good coverage across the model. The four receivers are located around the anomalous bodies. For each transmitter-receiver pair, an apparent resistivity is calculated and assigned to the transmitter location. These apparent resistivities are contoured, producing a map for each receiver (Figure 4).

The two models show different apparent resistivity maps, with the model containing the shallow more conductive anomaly yielding lower apparent resistivities. It is also important to notice that the receivers located on top of the anomalous regions show responses most geometrically similar to the model structure.

The principal physics illustrated by these examples is that as the source is moved near a conductive body, the current is drawn into that body, and less current is directed elsewhere. The larger and more conductive the body, the larger the effect. The apparent resistivity is strongly affected when the source is positioned in the vicinity of a conducting body. Whether the apparent resistivity increases or decreases at a receiver depends on the relative position of the receiver to the source and the conductive body. With a series of well-placed receivers and with large spatial transmission coverage, reliable maps of apparent resistivity like those shown in

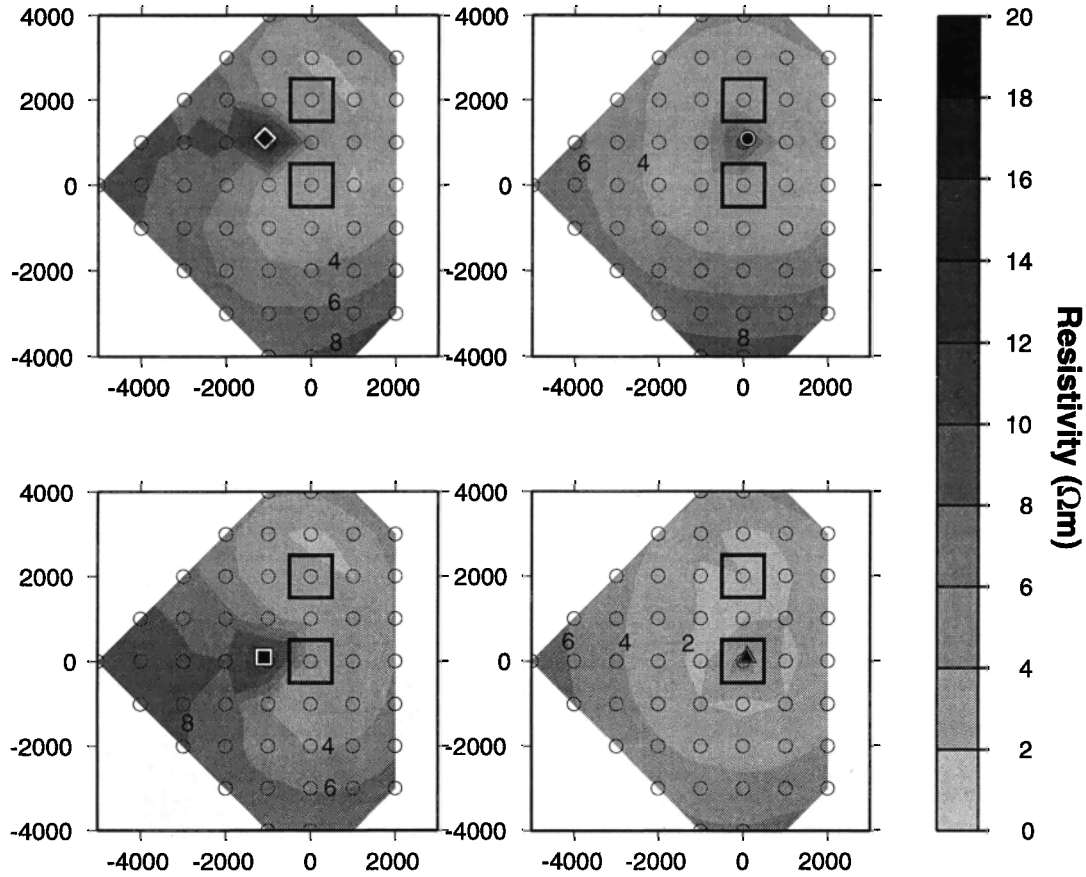

Figure 4a. Responses in terms of apparent resistivity maps for our first test model which considers a weak anomaly extending from 100 m to 1500 m depth below the seafloor. The responses are calculated at four different receiver sites (solid symbols). Transmitter locations are shown (open circles). Regions of hot convection are shown (open squares) and are 1 km by 1 km in lateral extent. Each plot is made by assigning an apparent resistivity value that is calculated at the receiver site to the location of the transmitter. Note that the biggest signal (reduction in apparent resistivities compared to the uniform 25 Ωm half-space) is seen by the instruments sited on top of the anomalies.

Figure 4 can be used to gain first-order insight into the subseafloor conductivity structure.

6. Experimental Procedure

The first stage of the experiment was to deploy remote seafloor magnetometers from the ship. The magnetometers used were of two types. Two of the ocean bottom magnetometers (OBM) used were developed at the University of Toronto and use a pair of fluxgate sensors to measure the horizontal component of the natural magnetic field at the seafloor. The other instrument, developed at Scripps Institution of Oceanography, has three orthogonal sensors, which form a tripod base on the seafloor. The coils are hung from an arm out to the side of the instrument during deployment. A release system drops the coils onto the seafloor after the instrument lands. The magnetometer sensors are separated from the recording package to reduce noise from tilting due to bottom currents. The magnetometer coils are simple windings over a ferrite core of about 0.5 m in total length and are installed in aluminum pressure housings. The magnetometer coils provide an output voltage that is proportional to magnetic field variation in a frequency band from 1 mHz to 30 Hz.

The locations of the magnetometers are shown in Figure 5. Instrument WHITE, the three-component Scripps device, was deployed on the NVZ of the northern Cleft segment at a water depth of 2260 m. OBM-1 was deployed 1000 m to the northeast, farther along the NVZ and was closest to the site of a large recent pillow flow. OBM-2 was deployed 1300 m to the west of instrument WHITE, in 2350 m of water, and off the NVZ.

Once the receivers were in place, the transmitting source was deployed. The source consists of a ship board power supply, which converts the ships three phase supply to a pseudosquare wave output of chosen current. A transverter control is used to determine the period of the square wave. The output from the power supply is fed to the two electrodes that make up the bipole source. One electrode was attached to the end of a conducting cable and lowered to the seafloor: it was electrically connected to the power supply through

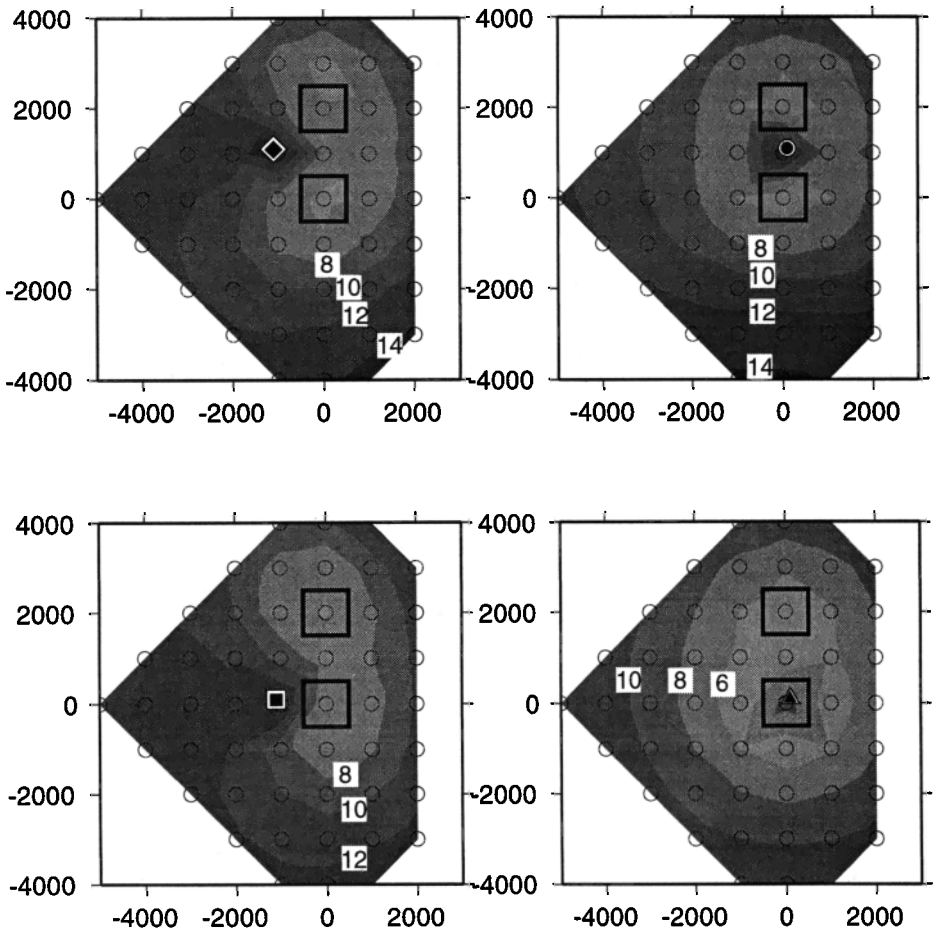

Figure 4b. As for Figure 4a except that a more conductive anomaly confined to the top 600 m of seafloor is considered.

slip rings on the winch drum. The other electrode was connected directly to the power supply, lowered over the side of the ship, and hung just below the seasurface. The electrodes were pieces of metal pipe about 1 m in length and 10 cm in diameter. The resistance of the electrodes is dependent on the length and surface area of the pipe and decreases as these increase. The current passing through the system was monitored by a Hall-effect sensor at the output of the power supply. A transponder was attached to the cable about 50 m above the seafloor electrode and gave positional information on the wire.

Once the lower electrode was in place just above the seafloor, a low-frequency waveform of 16 s period and 15 A current was passed between the electrodes. Because the inductive component of the magnetic field is small, the period of the transmitted signal is largely for convenience in the data processing, although *Nobes et al.* [1992] were able to usefully interpret the phase delays of the received signals.

The ship was held on station for 30 min so that a long time series was recorded on the receivers, improving the signal to noise ratio. On completion of a station, the wire was raised by about 30 m and the ship was moved to the next site. Once on station, the wire was allowed to become as close to vertical as possible before relowering it to the seafloor, so that the source is truly a vertical bipole.

7. Data Analysis

Thirty-four transmission stations were completed (Figure 5), with data collected on the three ocean bottom magnetometers. Most of the stations were placed along one line parallel to strike and one across strike running more or less through the middle of the OSC. Additional stations were added between these lines to give good azimuthal coverage. Simultaneous measurements of the horizontal magnetic field data were made at a land station at Ocean Beach in northern Washington. By rotating the land data and maximizing coherence between the land and seafloor time series, we are able to orient the seafloor magnetometers to within about 10°.

Time series during which the transmitter was operational are picked and Fourier transformed. The amplitude of the 16 s harmonic is examined, and if it is more than a factor of 2 above the adjacent harmonics, the value is regarded as data. In most cases, the signal

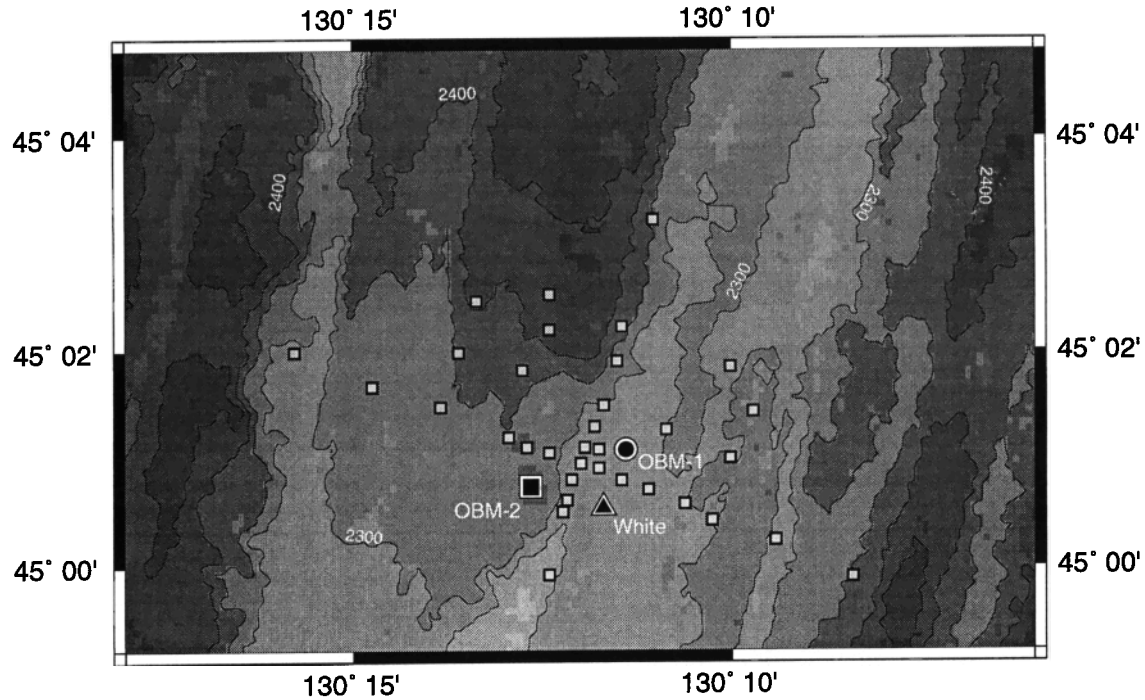

Figure 5. A closeup map of the survey area showing the positions of the three seafloor magnetometers as labeled (solid symbols). Also shown are the 34 transmission stations completed during the 3 day experiment (open squares). Each station took about an hour to complete, 30 min of which was spent transmitting.

amplitude is at least an order of magnitude larger than background noise, and data were recorded out to ranges of at least 5 km. On OBM-2, the amplitudes from each channel were combined geometrically to produce an estimate of the maximum horizontal magnetic field value. Instrument WHITE is a three component magnetometer with each of the sensors part of a tripod which are at an angle to the seafloor. We rotated the signals to determine the maximum magnetic field value. Over a layered Earth, the MMR source produces no vertical magnetic field, and modeling experience shows that the vertical field is always at least an order of magnitude smaller than the azimuthal component. Therefore we have used this maximum value to represent the horizontal field due to the source. The orientations obtained from land data were of particular importance for OBM-1 on which only one component of magnetic field was measured. By knowing the orientation of the receiver on the seafloor and the azimuth of the transmitter, we are able to estimate the maximum azimuthal component of the transmitted magnetic field. In this case, we assume that the azimuthal component of the magnetic field, which over a layered Earth is the only component produced, is the maximum component of the seafloor magnetic field. In the presence of three dimensionality, a radial component of magnetic field is produced, although it is generally significantly smaller (by about an order of magnitude) than the azimuthal component.

Global Positioning System (GPS) fixes of the instrument deployment position are assumed for the receiver seafloor locations. Averages of the ships position throughout the 30 min transmission windows were used to locate the transmitter. Variations in the ships position during each transmission period were typically less than 100 m.

We have most confidence in the data measured by instrument WHITE which is a three component device. OBM-1, for which only one component of magnetic field was recorded, is the least reliable: a 5° uncertainty in orientation can result in major uncertainties in the predicted azimuthal magnetic field, especially for stations at which the one component recorded points toward the transmitter. We have removed from consideration stations on OBM-1 for which the uncertainty in amplitude is greater than approximately 50% on the basis of orientation geometry.

8. Modeling

If the seafloor underlying the survey had a layered resistivity structure, then data collected on different instruments would exhibit the same amplitude-range characteristics, and would be indistinguishable from one another. The recorded amplitudes are shown in Figure 6, with data from each instrument assigned a different symbol. It is immediately apparent that an assumption of one dimensionality is untenable as the data from each instrument display markedly different behavior. The data collected on instrument WHITE (triangles), which was at the northern end of the Cleft seg-

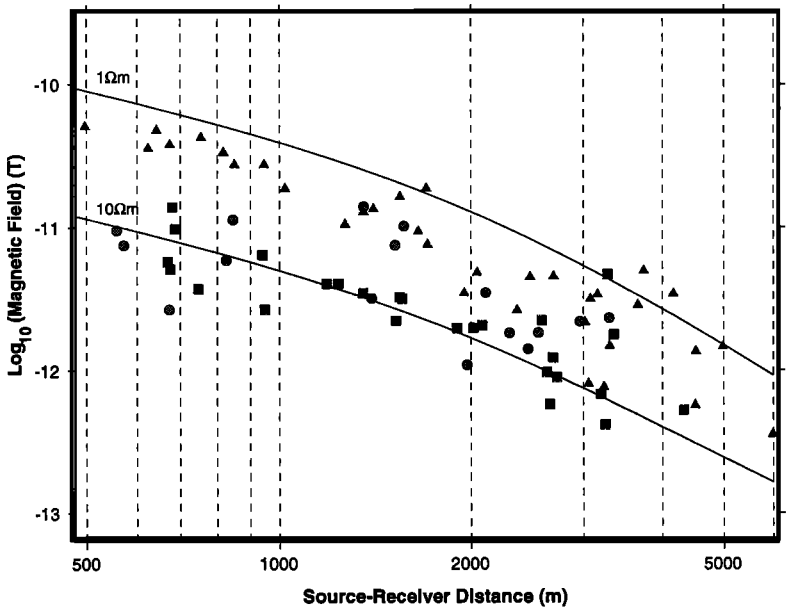

Figure 6. The magnetic field amplitude data collected on the three seafloor magnetometers. The data for each symbol are plotted using the same symbols as for the instrument location in Figure 5 (Instrument WHITE, triangles; OBM-1, circles; OBM-2, squares). The data for instrument WHITE show higher amplitudes, indicative of a less resistive seafloor than the other instruments. The difference in the responses between the instruments cannot be explained by a simple layered model of seafloor resistivity. The differences between the data on each instrument is exemplified by the responses of uniform half-spaces of values 1 Ωm and 10 Ωm shown as solid lines.

ment, have generally higher amplitudes, particularly at ranges less than 2 km. OBM-2 (squares) shows amplitudes which are smaller by a factor of approximately 5 at ranges of around 1 km. OBM-1 (circles) displays a more complex behavior, with occasional high amplitudes similar to those of instrument WHITE. At ranges greater than 2 km the dichotomy between instruments is less apparent, although instrument WHITE generally displays larger amplitudes for a given range.

It is easy to demonstrate the differences between the data on each instrument by comparing the measured amplitudes against half-space curves for different seafloor resistivities (Figure 6). The data on instrument WHITE are clearly more compatible with a 1 Ωm seafloor, while those on OBM-2 fall closer to the 10 Ωm half-space. This result remains true even if more formal methods of partitioning the amplitudes from each instrument into range bins, using the scatter in the data to generate error estimates, and inverting for a smooth layered-Earth structure [e.g., *Constable et al.*, 1987] are followed.

The differences in amplitudes recorded on each instrument or the scatter seen in amplitudes on a single instrument are not the result of random variations, either in the seafloor resistivity or in experimental geometry. Scatter in measurements of the seafloor electric field from controlled sources has been reported [*Evans et al.*, 1991, 1994], but the electric field is known to be distorted even by quite small-scale conductivity anomalies on which charges accumulate. The integrative nature of the magnetic field described above means that measured amplitudes are influenced only by features which have at least two dimensions that are a significant fraction of the source-receiver separation. The size of the scatter estimated from the residuals between the original data and one-dimensional best fit inversions is significantly larger than errors predicted from geometric uncertainties in the experimental configuration.

The observed amplitude behavior is caused by regional three dimensionality in the seafloor resistivity structure, and we demonstrate this by examining the areal behavior of the data, information which simple amplitude-range plots discard. For instrument WHITE, in which we have the best spatial coverage of the full magnetic field, we plot the data in terms of apparent resistivity calculated for each station and receiver. A triangulated contour map is built with the values of measured apparent resistivity placed at the transmitter location (Figure 7).

The apparent resistivity map for instrument WHITE (Figure 7), which was situated on the Cleft NVZ close to the site of known recent pillow flows, features two regions of low apparent resistivity (1 Ωm) embedded in more resistive surroundings. The two regions of low apparent resistivity coincide with the NVZs of the Cleft and Vance segments. The low-resistivity region beneath

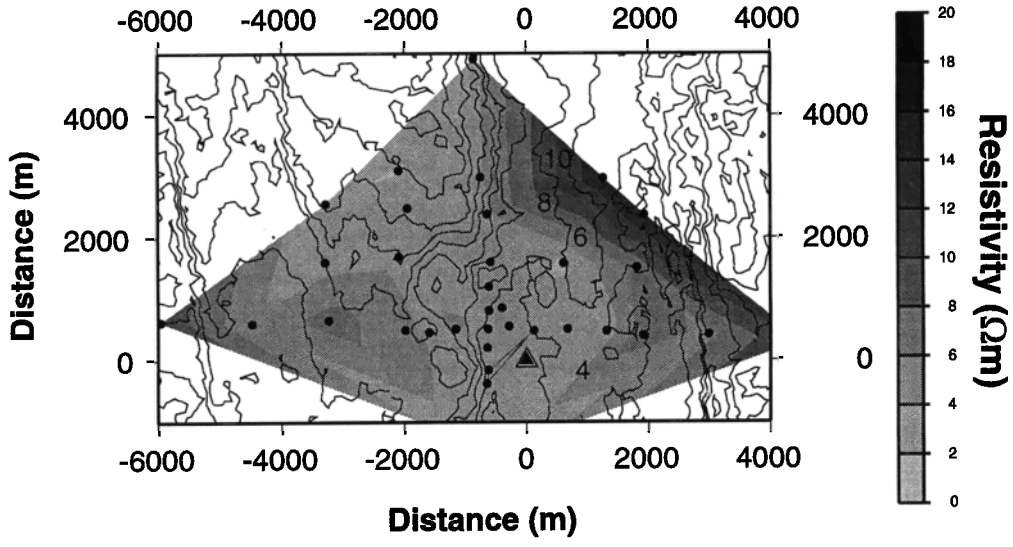

Figure 7. Map of apparent resistivity for instrument WHITE. The high magnetic field amplitudes measured by instrument WHITE and the spatial pattern of apparent resistivities observed lead us to believe that this receiver was situated on top of a region of anomalous resistivity and so is a particularly useful guide to the regional structure. The other two instruments have maps which are more difficult to interpret because the instruments are offset from the anomalous regions but most importantly because they recovered less complete coverage across the region and for this reason are not shown. The interactions between the source and the anomalous regions are complex and depend not only on the source-body geometry, but also on where the field is measured.

the Cleft segment is about 3 km in strike length and 2 km in maximum across-axis dimension. The anomaly ends 2 km to the north of the instrument location. The anomaly beneath the Vance appears to be slightly broader (3 km) in across-axis extent, overlaps the Cleft anomaly along strike by about 500 m, but is offset by about 1 km to the west. Data coverage does not place constraints on the southern extent of the Cleft anomaly nor on the northern extent of the Vance anomaly. However, the Cleft anomaly truncates well before the end of the line of recent pillow flows, which have been mapped further north into the OSC.

Apparent resistivity maps for the other two instruments show less of an obvious pattern, due partly to greater uncertainty on the magnetic field derived from one or two component data. The data are generally more resistive, reflecting lower measured magnetic field amplitudes.

In an attempt to explain the observed apparent resistivities in terms of subseafloor resistivity distributions, we have undertaken three-dimensional modeling, calculating the responses of bodies of anomalous resistivity buried in a uniform half-space. The numerical routine uses the MUDPACK finite difference algorithms [*Adams*, 1989, 1991] to calculate all components of the seafloor magnetic field and is described in detail in the Appendix. The modeling algorithm is nonlinear and computationally expensive and precludes the implementation of a reasonable inversion procedure. The computation is made more expensive because in the presence of three-dimensional structure reciprocity fails: this means that each time we move the source position, a new forward solution must be computed as the interaction terms between the source and anomalous structure are different.

The results we present below are based on forward modeling. In obtaining our preferred model, we examined the responses of a variety of classes of models containing conductors of different sizes beneath the ridge segments and OSC. Our model search was based closely on the existing seismological, magnetic, and gravity data as well as on the geological and hydrothermal observations made along the Cleft and Vance segments. While our final preferred model is nonunique, we have attempted through our modeling process to eliminate competing models of ridge electrical structure, so that our inferences of hydrothermal processes are as meaningful as possible.

We first considered the layer 2A thickness variation pattern reported by *McDonald et al.* [1994] as a basis for an electrical model. Our assumption was that a thick layer 2A consisting of heavily fractured pillow basalts and sheet flows would constitute a more conductive region due to its higher porosity. Therefore an electrical representation of the seismic layer 2A model would have a conductive body running through the middle of the OSC. Through examination of the apparent resistivity map for instrument WHITE, as well as the results of a series of models placing a conductive body through the middle of the OSC, we discount this struc-

ture as providing an explanation for our data. Such a model fails to account for most of the data features: it does not show reduced apparent resistivities beneath the NVZs for instrument WHITE, and it does not reproduce the splitting in amplitudes seen between the instruments at short ranges. The fact that we see the most conductive regions beneath the ridge-axis, where layer 2A is predicted to be thinnest, suggests that in the uppermost crust our data are responding primarily to variations in the pore water temperature rather than its volume.

Next, we constructed models containing a variety of conductive anomalies beneath the NVZ of the two ridge segments and used trial and error forward modeling to arrive at a preferred model.

Our preferred model mirrors the apparent resistivity map shown for instrument WHITE and is shown in Figure 8 along with a synthetic apparent resistivity map for this instrument. Amplitude responses of this model for all instruments are shown in Figure 9. The model contains two conductive bodies within the uppermost 1 km of crust beneath the NVZs of both the Cleft and Vance segments.

Beneath the Cleft segment, we include a conductive body within the uppermost 1 km of seafloor with a resistivity of (0.29 Ωm). The conductive anomaly beneath the Vance segment is broader in across axis dimension than that beneath Cleft, and has a slightly higher resistivity (0.4 Ωm). The Cleft anomaly does not appear to extend any further north than the position of OBM-1. Our data coverage does not allow us to constrain the northern extent of the Vance anomaly. Our background resistivity is a uniform half-space of 16 Ωm.

In general, our preferred model predicts the shape and amplitude of the instrument WHITE response well (Figure 8) as well as other features of the amplitude data on the other instruments (Figure 9). The RMS misfit between instrument WHITE data and the model response is less than 1.0 assuming uniform 10% errors in the amplitude estimates. In general, we believe an uncertainty of 100 m in range corresponds to about a 10% uncertainty in amplitude, while the three-dimensional modeling code has been shown to be accurate to within 10%. The model reproduces quite well the splitting in amplitudes seen between instrument WHITE and OBM-2 to ranges of around 2 km. The model therefore achieves a major improvement in fit over a layered model, not only in terms of overall misfit but also in terms of residuals and bias between the data and responses of all instruments. The misfits for OBM-1 and 2 are also close to the expected RMS value of 1.0 assuming Gaussian errors of 15% and are certainly within 1.0 if 20% errors are assigned.

The two receivers which show resistive responses do so because they are not on top of the conductive bodies but are offset from them. The complex form of these instrument's responses may result from interactions which are beyond the ability of our code to reproduce. Our model response does predict the observed differences in amplitudes between instruments WHITE and OBM-2 to ranges of about 2 km, but we were unable to fit the more apparently complicated pattern at larger range for OBM-2. The instrument WHITE response which was collected on top of the conductive anomaly is more coherent and is probably the most reliable indicator of the bulk regional structure.

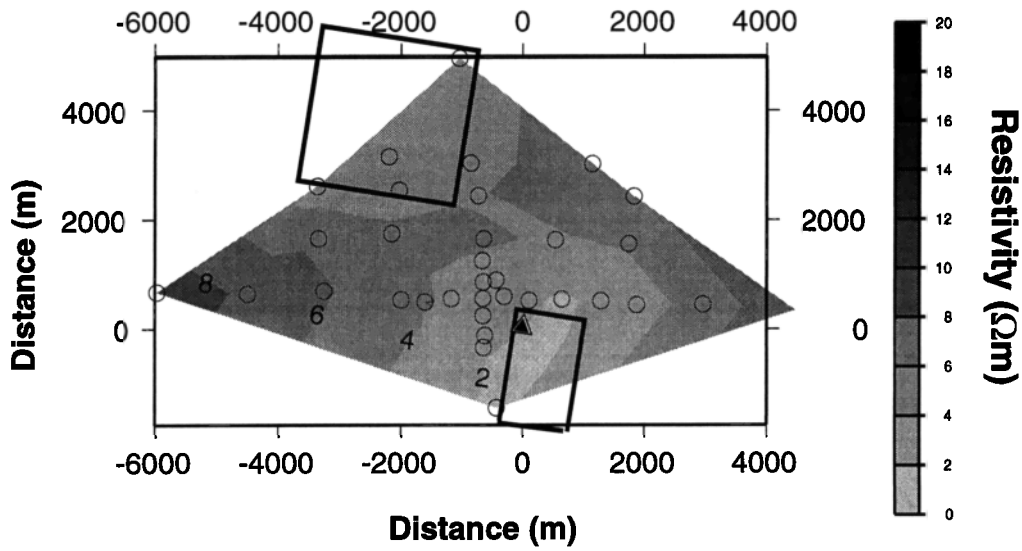

Figure 8. The response of our preferred model of OSC electrical structure shown as an apparent resistivity map for instrument WHITE. The outlines of the two conductive bodies inserted in the model are shown. The body beneath the Cleft NVZ has a resistivity of 0.29 Ωm (conductivity 3.5 S/m) and extends from about 100 m to 600 m below the seafloor. The body beneath the Vance segment is less conductive (2.5 S/m, 0.4 Ωm) but has the same vertical extent. The surrounding seafloor is modeled by a half-space of 16 Ωm.

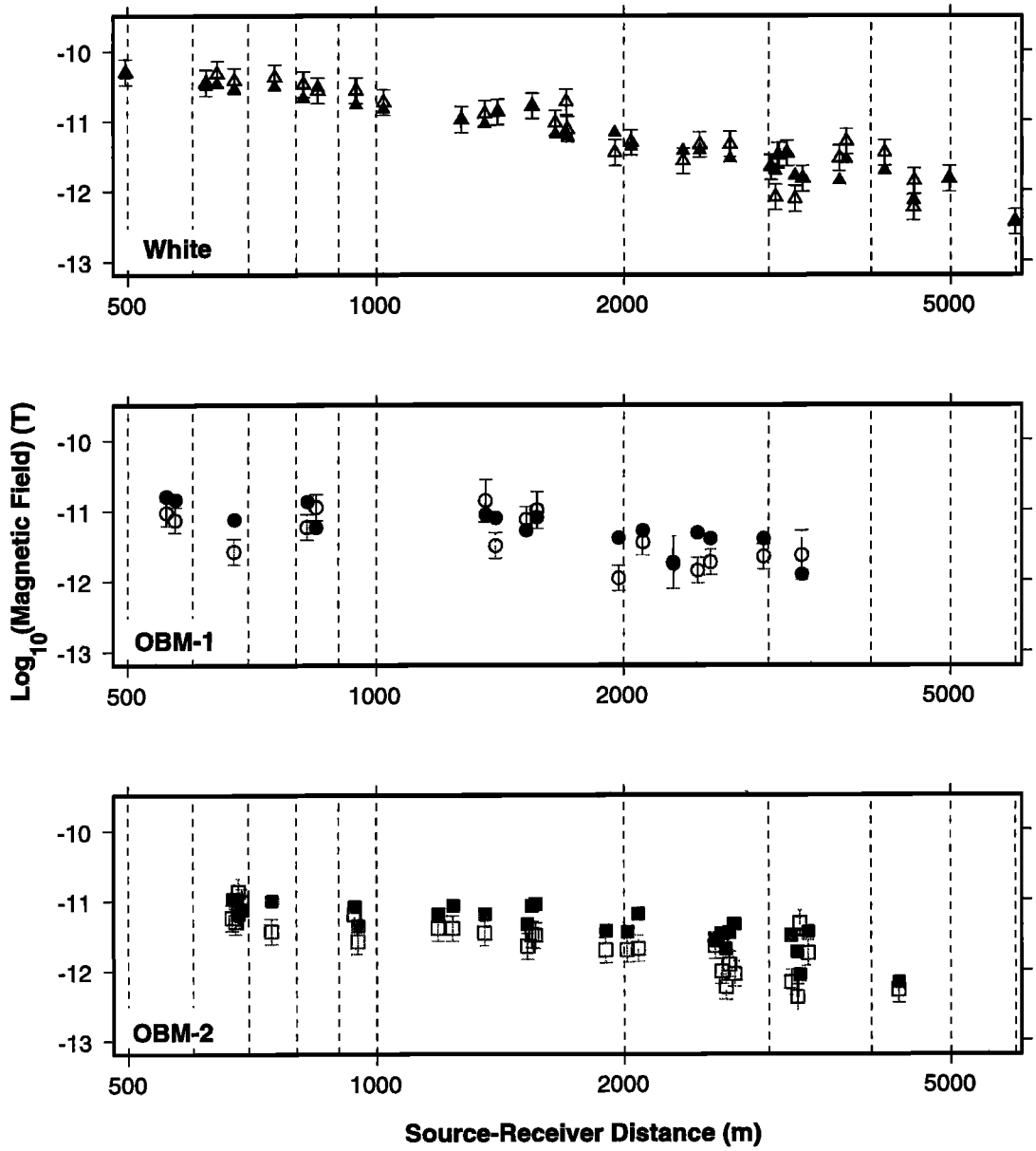

Figure 9. The response of our preferred model in terms of the magnetic field for each instrument. The response (solid symbols) and the respective data (outlined symbols with error bars) are shown. The deviations in response from a simple falloff with range is due to the three-dimensional structure in the model. All symbols are as in Figure 6. Error bars of 20% have been added on the basis of our best predictions of combined sources of uncertainty. For OBM-1, larger error bars account for the fact that this instrument only recorded a single component of magnetic field. Note that the model not only predicts the raised amplitudes for instrument WHITE (triangles) but also reproduces the split in amplitudes, thus representing a substantial improvement over layered models.

9. Temperature and Porosity Profiles

Vertical cross sections through our preferred model show that conductivities beneath the Cleft and Vance segments are comparable to that of seawater at ambient seafloor temperatures. Given reasonable estimates of crustal porosity structure, this requires raised crustal temperatures, enhancing the pore fluid conductivity. The size of the maximum thermal anomaly beneath the Vance seems to be lower than that beneath Cleft based on the different conductivities seen in the two regions (3.5 S/m (0.29 Ωm) beneath Cleft versus 2.5 S/m (0.4 Ωm) beneath Vance).

There is substantial nonuniqueness associated with temperature and porosity estimates obtained from resistivity measurements. Rather than convert resistivity values to porosity (ϕ) or temperature (T) in a piecewise and independent sense, we have treated ϕ and T as functions of depth. We have produced ϕ and T profiles for the Cleft and Vance axes, as well as off-axis, by impos-

ing gradient constraints so that T is forced to increase with depth and ϕ to decrease. Both ϕ and T are represented by cubic polynomial functions of depth, making the imposition of gradient constraints straightforward. We have used a simple grid search through model space to find the optimum combination of profiles which predict the observed resistivity profiles. The pore water conductivity was determined using the available laboratory data described above [*Nesbitt*, 1993; *Quist and Marshall*, 1968], but we have assumed a normal seawater salinity.

The upper crustal density values reported by *Stevenson et al.* [1994] in the OSC predict a porosity of about 17%, and we have used this value as a tie point at the seafloor in the inversion process. We also constrain temperatures to be below 1100°C, approximately the melting temperature of basalt at crustal pressures. Since we have good reason to expect the seafloor on axis to be cracked, we have used an exponent of 1.2 in *Archie*'s [1942] law, in keeping with the results of *Evans* [1994] for the EPR. Off-axis, there is evidence to suggest a degree of unconnectedness in the fluid distribution, as a connected fluid distribution of 16 Ωm resistivity predicts a porosity of around 4% at ambient seafloor temperatures rather than the 17% inferred from gravity data. If crack closure has occurred, so that a higher exponent in Archie's law is required, then it is possible to sustain a higher porosity and still see higher resistivities. We find that an exponent of 2.0 results in temperature and porosity profiles which are a closer fit to the resistivity values.

Two profiles of ϕ and T, one for the Cleft NVZ and the other for off-axis, along with their predicted resistivity profiles compared to the model are shown in Figure 10. A word of caution is that these profiles do not allow sharp discontinuities in either T (i.e., a sharp transition from primarily convective to advective transport) or porosity (i.e., a sharp boundary in lithology) and so should be interpreted accordingly.

Our models show similar characteristics to the resistivities predicted from the simple convection model of *Wilcock* [1997] combined with estimates of crustal porosities [*Stevenson et al.*, 1994; *Becker*, 1985; *Becker*, 1989]. The rapid increase in resistivity away from the ridge axis is also predicted by, amongst others, models 4 and 5 of *Sleep* [1991], which have narrow bands of high temperatures focused within 1 km of the ridge axis, extending throughout the uppermost 1 km or so of crust. This model is generally consistent with our model except that the bands of high temperature are narrower than we predict (although Sleep notes that extension of vent conduits a finite distance away from the ridge axis would widen the predicted hot zones). Recharge of cold seawater into the system would occur a few kilometers off-axis under this flow regime. The influence of cracked-induced permeability on hydrothermal circulation has been studied by *Yang et al.* [1996] for sediment-covered systems, and the presence of cracks is shown to initiate and maintain subcritical convection in cells of aspect ratio 1.7-2.0, broadly consistent with our observation. We are not able to identify whether circulation is predominantly across-strike, as in these two-dimensional numerical models, or along strike as proposed by other workers based on geological observations [e.g., *Nehlig*, 1993; *Haymon et al.*, 1991]. The lack of seismic constraints on magma chamber geometry make inference of the relationships between driving heat source and hydrothermal circulation patterns impossible.

10. Summary

Standard geophysical methods have been unable to provide constraints on regions of active hydrothermal circulation within the uppermost crust at mid-ocean ridges. On the basis of the results of an MMR electromagnetic survey, we have demonstrated that the crustal resistivity in the Cleft-Vance OSC is controlled by the thermal structure and not by porosity variations associated with the development of a mature extrusive pile, or layer 2A as it is known seismically. Our preferred model of crustal resistivity includes two bands of low resistivity approximately 2 km wide extending to a depth of around 1 km below both NVZs of the Cleft and Vance segments (Figure 10). We believe that the reduced resistivities beneath Cleft are associated with hot seawater percolating through the porous upper crust. This belief is supported by submersible and camera-tow observations of high temperature venting and diffuse flow coincident with one of our regions of low resistivity [*Embley and Chadwick*, 1994].

Numerical models of hydrothermal circulation [*Sleep*, 1991] are generally consistent with the electrical measurements, supporting our conclusion that the width of the shallow band of low resistivity is controlled by the thermal regime at the ridge crest and varies rapidly in temperature away from the ridge crest. Sleep inferred a depth extent for hydrothermal fluids to about 0.8 km above the magma chamber. The width of the hot hydrothermal zone varied with the details of the models, but a width of 1.5-2 km was consistent with some models. Our data coverage is too sparse to constrain the shape of the hydrothermal zone in any detail. Furthermore, the resistivity models are only able to provide constraints on crust at temperatures less than about 350°C. However, we do see that the northernmost extent of circulation beneath the Cleft segment ends approximately at the location of a large, fresh pillow flow, noted as flow 1 by *Chadwick and Embley* [1994]. The circulation does not extend farther northward along the line of other smaller flows which have been mapped during submersible dives and camera tows.

Seismic refraction data collected farther north within the CoAxial valley by *Sohn et al.* [1997] indicate similar rapid changes in seismic properties within a few kilometers of the ridge axis. What is unusual about the Sohn

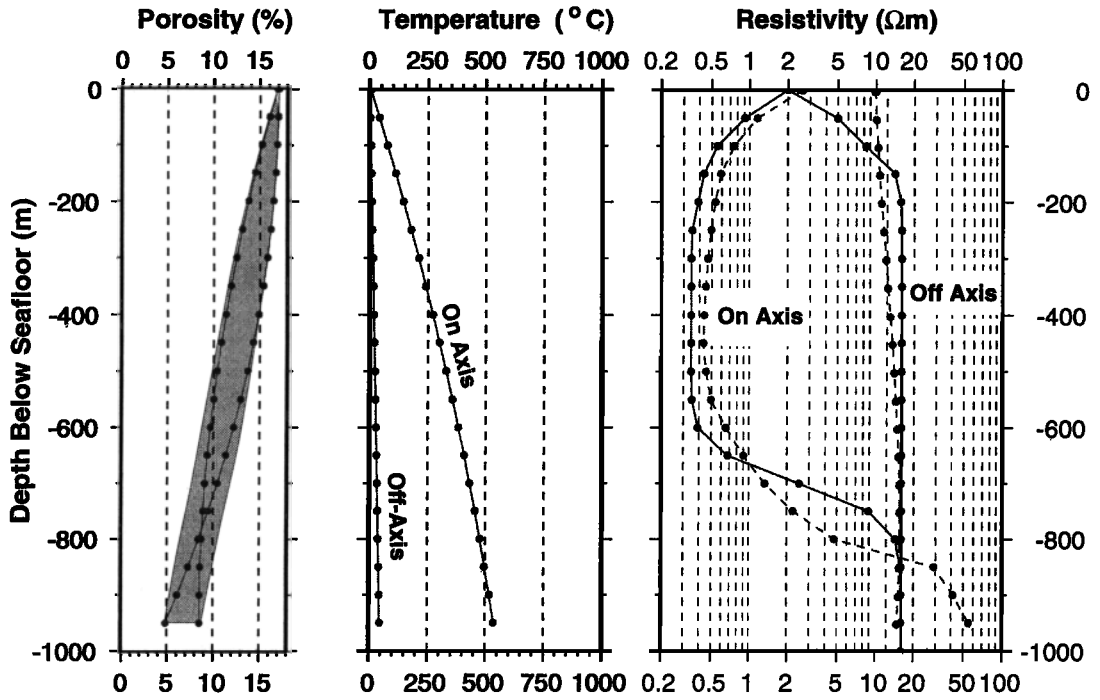

Figure 10. Vertical cross sections through the anomalous bodies of Figure 8 showing the distribution of resistivities beneath the Cleft NVZ and off-axis. We have inverted these resistivity depth profiles for T and ϕ profiles using the method described in the text. (right) The resistivity profiles predicted by the T and ϕ profiles are also shown (dashed lines). The vertical section through the Vance NVZ is similar in vertical extent to that beneath Cleft, except that the maximum conductivity is only 2.5 S/m (0.4 Ωm). We relate the shallow anomalies to a zone of hot percolating hydrothermal fluids. The axial profile is consistent with an upwelling region of fluid at temperatures below 350°C, similar in structure to that shown in Figure 3 [*Wilcock*, 1997]. The off-axis profile requires either a degree of crack closure (or else a reduction in porosity) but also points to lower crustal temperatures.

et al. model is that within the axial valley the shallow porosity decreases away from the axis, as cracks responsible for hydrothermal circulation become sealed by depositional products, but then increases again as off-axis faulting reopens these cracks and generates new ones. This model is compatible with our observations, except that in our case, we must also recognize the effects of temperature on the resistivity structure. A model in which hydrothermal circulation is confined to a narrow axial zone, a few kilometers wide, which cools rapidly, and in which cracks are sealed, will result in the sharp increase in resistivity seen off-axis, although our model also requires some crack closure off-axis.

We note that the conductive bodies beneath the Cleft segment overlap at most the first few documented flows in the 17 km trail of fresh pillow flows [*Embley and Chadwick*, 1994]. This observation is evidence to support the model proposed by *Embley and Chadwick* in which these flows are the result of a dike intrusion, which propagated along the NVZ rather than from a magma source underlying the entire northern part of the segment. The intrusion responsible for this must have cooled rapidly and sufficiently so that it no longer has an impact on the shallow resistivity structure. Observed high-temperature venting is also confined within the boundaries of our shallow conductive anomaly. To date, we know of no supporting evidence for hydrothermal activity at the southern reaches of the Vance segment.

The results in this paper represent a first attempt at constraining the thermal state of the crust using the MMR method. While the results are encouraging, in that we have delineated regions of elevated temperature, tighter constraints will require a larger number of three component magnetometers throughout the survey area as well as good controls on crustal structure from seismic methods.

Appendix: Calculation of Response of Anomalous Bodies of Finite Size

In order to quantify the effects of buried features of finite size on our data, we solve for the steady state (DC) anomalous fields generated by such a body buried in a uniform half-space.

Consider the normal fields, E_n and B_n, in the absence of any anomaly and the total fields when an anomaly is present, E_t and B_t.

For the static case, the normal fields are given by

$$\nabla_\wedge B_n = \mu_o(J_n + J_n^s) \quad \text{(A1)}$$

$$\nabla_\wedge E_n = 0 \quad \text{(A2)}$$

where J_n^s are the source currents.
The total fields are given by

$$\nabla_\wedge B_t = \mu_o(J_t + J_n^s) \quad \text{(A3)}$$

$$\nabla_\wedge E_t = 0 \quad \text{(A4)}$$

In this case, the total conductivity of the Earth, σ_t, is given by

$$\sigma_t = \sigma_a + \sigma_n \quad \text{(A5)}$$

where σ_a is the conductivity of the anomaly and σ_n is the background conductivity.

We can subtract the normal fields from the total fields to give expressions for the anomalous fields, which are independent of the source terms. Combining the resulting pair of expressions for E_a and B_a yields

$$\frac{1}{\mu_o}\nabla^2 B_a = E_a \nabla_\wedge(\nabla\sigma_t) + E_n \nabla_\wedge(\nabla\sigma_a) \quad \text{(A6)}$$

Thus we have three coupled expressions involving each component of the anomalous electric and magnetic fields, with the normal electric field components known: we have assumed that the surrounding medium is a uniform double half-space. We choose a Cartesian coordinate system as the most convenient for solution.

We have used the finite difference MUDPACK routines [*Adams*, 1989, 1991] to solve the above system of differential equations in an iterative fashion. We assume that the anomalous electric fields are zero everywhere and obtain a first guess for the anomalous magnetic field components. This first guess is then used in the intermediate expression

$$\nabla_\wedge B_a = \mu_o\{\sigma_a E_n + (\sigma_n + \sigma_a)E_a\} \quad \text{(A7)}$$

to obtain a first guess for the anomalous electric fields, and an iterative loop is established.

The formulation of the finite difference scheme requires the evaluation of the derivatives of conductivity at all points on the grid, precluding us from using discrete conductivity blocks. Anomalous prisms are established by defining the center of the body, its dimensions in grid units in each of the three Cartesian directions, and a maximum conductivity value. Each anomalous body is then blended continuously into the background by the use of hyperbolic tangent functions, which can be controlled by coefficients to allow a sharp or gradual change in conductivity at the boundaries of the body. We use derivative boundary conditions by assuming that far from the anomaly the field produced by its interaction with the source has a dipole behavior and falls off with range, accordingly.

Tests on the code have been conducted using a sheet-like buried anomaly, which mimics a conductive layer. A solution volume of 12 km by 12 km by 3 km vertically was discretized into a 97x97x65 grid. Two anomalous bodies were included in the model: the first (0.33 Ωm) was buried at a depth of 200 m and had a vertical extent below this depth of 500 m and the top of the second body (0.25 Ωm) was at 1700 m depth and also had a vertical extent of 500 m. Both bodies had lateral extents the same as the solution volume in both x and y directions, so that the model constructed mimicked a layered Earth. The surrounding seafloor was a uniform half-space of 5 Ωm. The solution from the three-dimensional code was compared to the layered Earth solution described by *Edwards et al.* [1981], which is easily computed. At ranges greater than about 500 m from the source and to the ranges of around 5-6 km in which we are interested, the two solutions agree to within 10% in terms of apparent resistivity. The solution does less well closer to the boundary of the model. We regard the sheet like anomaly as a fairly stringent test of our code, particularly in terms of the boundary behavior, and feel confident that the 10% uncertainty level is reasonable once the bodies we represent are smaller in size than the solution volume.

Acknowledgments. We would like to thank the captain and crew of the R/V New Horizon for their help during the cruise. Ship time for this experiment was provided under an NSERC grant to R. Nigel Edwards who we thank for his help and support. Bob Embley provided helpful discussion and access to unpublished data on the Cleft-Vance geology. We appreciate the helpful reviews from Cathy Constable, as associate editor, Hjalmar Eysteinsson, and one anonymous reviewer. Comments from Meg Tivey also helped the clarity of the paper. Support for data analysis was provided by NSF grant OCE-9503130, by the J. Lamar Worzel Assistant Scientist Fund, (Palisades Geophysical Institute), and by the Penzance Endowed Fund in Support of Scientific Staff. WHOI contribution number 9685.

References

Adams, J.C., MUDPACK: Multigrid portable FORTRAN software for the efficient solution of linear elliptic partial differential equations, *Appl. Math. Comput.*, *34*, 113-146, 1989.

Adams, J.C., Recent enhancements in MUDPACK: A multigrid software package for elliptic partial differential equations, *Appl. Math. Comp.*, *43*, 79-93, 1991.

Alt, J.C., J. Honnorez, C. Laverne, and R. Emmermann, Hydrothermal alteration of a 1 km section through the upper oceanic crust, Deep Sea Drilling Project hole 504B: Mineralogy, chemistry, and evolution of seawater-basalt interactions, *J. Geophys. Res.*, *91*, 10,309-10,335, 1986.

Archie, G.E., The electrical resistivity log as an aid in determining some reservoir characteristics, *J. Pet. Technol.*, *5*, 1-8, 1942.

Baker, E.T., G.J. Massoth, and R.A. Feely, Cataclysmic venting on the Juan de Fuca Ridge, *Nature*, *329*, 149-151, 1987.

Baker, E.T., W. Lavelle, R.A. Feely, G.J. Massoth, and S.L. Walker, Episodic venting on the Juan de Fuca Ridge, *J. Geophys. Res.*, *94*, 9237-9250, 1989.

Becker, K., Large-scale electrical resistivity and bulk porosity of the oceanic crust, DSDP hole 504B, Cost-Rica rift. *Initial rep. of Deep Sea Drill. Proj.*, *83*, 419-427, 1985.

Becker, K., Measurements of the permeability of the sheeted dikes in hole 504B, *Proc. Ocean Drill. Program Sci. Results*, *111*, 317-325, 1989.

Bischoff, J.L., and R.J. Rosenbauer, An empirical equation of state for hydrothermal seawater (3.2% NaCl), *Am. J. Sci.*, *285*, 725-763, 1985.

Chadwick, W.W., Jr., and R.W. Embley, Lava flows from a mid-1980s submarine eruption on the Cleft segment, Juan de Fuca Ridge, *J. Geophys. Res.*, *99*, 4761-4776, 1994.

Chave, A.S., S.C. Constable, and R.N. Edwards, Electrical exploration methods for the seafloor, in *Electromagnetic Methods in Applied Geophysics*, vol. 2, *Applications*, edited by M. Nabighian, pp. 931-966, Soc. of Explor. Geophys. Tulsa, Okla., 1991.

Christeson, G.L., G.M. Purdy, and G.J. Fryer, Structure of young upper crust at the East Pacific Rise near 9°30′N, *Geophys. Res. Lett.*, *19*, 1045-1048, 1992.

Constable, S.C., R.L. Parker, and C.G. Constable, Occam's inversion: A practical algorithm for generating smooth models from electromagnetic sounding data, *Geophysics*, *52*, 289-300, 1987.

Cox, C.S., S.C. Constable, A.D. Chave, and S.C. Webb, Controlled source electromagnetic sounding of the oceanic lithosphere, *Nature*, *320*, 52-54, 1986.

Delaney, J.R., D.W. Mogk, and M.J. Mottl, Quartz cemented breccias from the mid-Atlantic Ridge: Samples of high-salinity hydrothermal upflow zone, *J. Geophys. Res.*, *92*, 9175-9192, 1987.

Edwards, R.N., L.K. Law, and J.M. Delaurier, On measuring the electrical conductivity of the oceanic crust by a modified magnetometric resistivity method, *J. Geophys. Res.*, *86*, 11,609-11,615, 1981.

Embley, R.W., and W.W. Chadwick, Jr., Volcanic and hydrothermal processes associated with a recent phase of seafloor spreading at the northern Cleft segment: Juan de Fuca Ridge, *J. Geophys. Res.*, *99*, 4741-4760, 1994.

Embley, R.W., S.R. Hammond, A. Malahoff, W.B.F. Ryan, K. Crane, and E. Kappel, Rifts of the southern Juan de Fuca (abstract), *Eos Trans. AGU*, *64*, 853, 1983.

Evans, R.L., Constraints on the large scale porosity of young oceanic crust from seismic and resistivity data, *Geophys. J. Int.*, *119*, 869-879, 1994.

Evans, R.L., S.C. Constable, M.C. Sinha, C.S. Cox, and M.J. Unsworth, Upper-crustal resistivity structure of the East Pacific Rise near 13°N, *Geophys. Res. Lett.*, *18*, 1917-1920, 1991.

Evans, R.L., M.C. Sinha, S.C. Constable, and M.J. Unsworth, On the electrical nature of the axial melt zone at 13°N on the East Pacific Rise, *J. Geophys. Res.*, *99*, 577-588, 1994.

Haymon, R.M., D.J. Fornari, M.H. Edwards, S. Carbotte, D. Wright, and K.C. Macdonald, Hydrothermal vent distribution along the East Pacific Rise crest (9°09′-54′ N) and its relationship to magmatic and tectonic processes on fast spreading midocean ridges, *Earth Planet. Sci. Lett.*, *104*, 513-534, 1991.

Kappel, E.S., and W.R. Normark, Morphometric variability within the axial zone of the southern Juan de Fuca Ridge: Interpretation from from Sea MARC II, Sea MARC I, and deep-sea photography, *J. Geophys. Res.*, *92*, 11,291-11,302, 1987.

Kappel, E.S., and W.B.F. Ryan, Volcanic episodicity and a non-steady state rift valley along northeast Pacific spreading centers: Evidence from Sea MARC I, *J. Geophys. Res.*, *91*, 13,925-13,940, 1986.

Kelley, D.S., K.M. Gillis, and G. Thompson, Fluid evolution in submarine magma-hydrothermal systems at the mid-Atlantic Ridge, *J. Geophys. Res.*, *98*, 19,579-19,596, 1993.

Kent, G.M., A.J. Harding, and J.A. Orcutt, Distribution of magma beneath the East Pacific Rise near the 9°03′ N overlapping spreading center from forward modeling of common depth point data, *J. Geophys. Res.*, *98*, 13,971-13,995, 1993.

Lonsdale, P., Overlapping rift zones at the 5.5°S offset of the East Pacific Rise, *J. Geophys. Res.*, *88*, 9393-9406, 1983.

Macdonald, K.C., J.-C. Sempere, and P.J. Fox, East Pacific Rise from the Siqueiros to Orozco fracture zones: Along strike-continuity of the axial neovolcanic zone and structure and evolution of overlapping spreading centers, *J. Geophys. Res.*, *89*, 6049-6069, 1984.

McDonald, M.A., S.C. Webb, J.A. Hildebrand, B.D. Cornuelle, and C.G. Fox, Seismic structure and anisotropy of the Juan de Fuca Ridge at 45°N, *J. Geophys. Res.*, *99*, 4857-4873, 1994.

Morton, J.L., N.H. Sleep, W.R. Normark, and D.H. Tomkins, Structure of the southern Juan de Fuca Ridge from seismic reflection records, *J. Geophys. Res.*, *92*, 11,315-11,326, 1987.

Nehlig, P., Interactions between magma chambers and hydrothermal systems: Oceanic and ophiolitic constraints, *J. Geophys. Res.*, *98*, 19,621-19,633, 1993.

Nehlig, P., and T. Juteau, Deep crustal seawater penetration and circulation at ocean ridges: Evidence from the Oman ophiolite, *Mar. Geol.*, *84*, 209-228, 1988.

Nesbitt, B.E., Electrical resistivities of crustal fluids, *J. Geophys. Res.*, *98*, 4301-4310, 1993.

Nobes, D.C., L.K. Law, and R.N. Edwards, The determination of resistivity and porosity of the sediment and fractured basalt layers near the Juan de Fuca Ridge, *Geophys. J. R. Astron. Soc.*, *86*, 289-317, 1986.

Nobes, D.C., L.K. Law, and R.N. Edwards, Results of a seafloor electromagnetic survey over a sedimented hydrothermal area on the Juan de Fuca Ridge, *Geophys. J. Int.*, *110*, 333-346, 1992.

Pezard, P.A., Electrical properties of mid-ocean ridge basalt and implications for the structure of the upper oceanic crust in hole 504B, *J. Geophys. Res.*, *95*, 9237-9264, 1990.

Quist, A.S., and W.L. Marshall, Electrical conductances of aqueous sodium chloride solutions from 0 to 800°C and at pressures to 4000 bars, *J. Phys. Chem.*, *71*, 684-703, 1968.

Rosenberg, N.D., F.J. Spera, and R.M. Haymon, The relationship between flow and permeability field in seafloor hydrothermal systems, *Earth Planet. Sci. Lett.*, *116*, 135-153, 1993.

Sleep, N.H., Hydrothermal circulation, Anhydrite precipitation, and thermal structure at ridge axes, *J. Geophys. Res.*, *96*, 2375-2387, 1991.

Sohn, R.A., S.C. Webb, J.A. Hildebrand, and B.D. Cornuelle, Three-dimensional tomographic velocity structure of upper crust, CoAxial segment, Juan de Fuca Ridge: Implications for on-axis evolution and hydrothermal circulation, *J. Geophys. Res.*, *102*, 17,679-17,695, 1997.

Stevenson, J.M., J.A. Hildebrand, M.A. Zumberge, and C.G. Fox, An ocean bottom gravity study of the southern Juan de Fuca Ridge, *J. Geophys. Res.*, *99*, 875-888, 1994.

Tivey, M.A., Fine scale magnetic anomaly field over the southern Juan de Fuca Ridge: Axial magnetization low and implications for crustal structure, *J. Geophys. Res.*, *99*, 4833-4857, 1994.

Travis, B.J., D.R. Janecky, and N.D. Rosenberg, Three-dimensional simulation of hydrothermal circulation at mid-ocean ridges, *Geophys. Res. Lett.*, *18*, 1441-1444, 1991.

Wilcock, W.S.D., A model for the formation of transient event plumes above mid-ocean ridge hydrothermal systems, *J. Geophys. Res.*, *102*, 12,109-12,121, 1997.

Wolfgram, P., R.N. Edwards, L.K. Law, and M.N. Bone, Polymetallic sulfide exploration on the deep sea floor: The

feasibility of the mini-MOSES experiment, *Geophysics*, *51*, 1808-1818, 1986.

Yang, J., R.N. Edwards, J.W. Molson, and E.A. Sudicky, Fracture induced hydrothermal convection in the oceanic crust and the interpretation of heat-flow data, *Geophys. Res. Lett.*, *23*, 929-932, 1996.

Young, P.D., and C.S. Cox, Electromagnetic active source sounding near the East Pacific Rise, *Geophys. Res. Lett.*, *8*, 1043-1046, 1981.

R.L. Evans, Department of Geology and Geophysics, Woods Hole Oceanographic Institution, Woods Hole, MA 02543. (email: revans@whoi.edu)

M. Jegen, Institute of Theoretical Geophysics, Downing Street, Cambridge, U.K. (email: jegen@esc.cam.ac.uk)

K. Sananikone, U.S. Geological Survey, Woods Hole, MA 02543. (email: khamla@carbon.er.usgs.gov)

S.C. Webb, Marine Physical laboratories, Scripps Institution of Oceanography, CA 92093. (email: scw@mpl.ucsd.edu)

(Received September 4, 1997; revised January 22, 1998; accepted February 2, 1998.)